Heliyon 10 (2024) e29483

Contents lists available at ScienceDirect

Heliyon

journal homepage: www.cell.com/heliyon

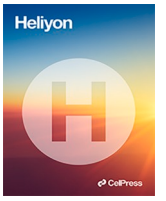

Research article

The protective effects of methylene blue on astrocytic swelling after cerebral ischemia-reperfusion injuries are mediated by Aquaporin-4 and metabotropic glutamate receptor 5 activation

Yu Lai [a,*,1], Jie Han [a,1], Dongxian Qiu [b], Xinyan Liu [c], Kan Sun [a], Yuzhu Fan [d], Chunliang Wang [a], Song Zhang [a]

[a] Department of Cardiovascular, The Traditional Chinese Medicine Hospital of Shijiazhuang, Shijiazhuang, 050011, Hebei, China
[b] Department of Dermatology, The Traditional Chinese Medicine Hospital of Shijiazhuang, Shijiazhuang, 050011, Hebei, China
[c] Medical Insurance Division, The Traditional Chinese Medicine Hospital of Shijiazhuang, Shijiazhuang, 050011, Hebei, China
[d] Department of Endocrinology, The Traditional Chinese Medicine Hospital of Shijiazhuang, Shijiazhuang, 050011, Hebei, China

ARTICLE INFO

Keywords:
Ischemic stroke
brain edema
Methylene blue
AQP 4
mGluR5

ABSTRACT

Methylene blue (MB) was found to exert neuroprotective effect on different brain diseases, such as ischemic stroke. This study assessed the MB effects on ischemia induced brain edema and its role in the inhibition of aquaporin 4 (AQP4) and metabotropic glutamate receptor 5 (mGluR5) expression. Rats were exposed 1 h transient middle cerebral artery occlusion (tMCAO), and MB was injected intravenously following reperfusion (3 mg/kg). Magnetic resonance imaging (MRI) and 2,3,5-triphenyltetrazolium chloride (TTC) staining was performed 48 h after the onset of tMCAO to evaluate the brain infarction and edema. Brain tissues injuries as well as the glial fibrillary acidic protein (GFAP), AQP4 and mGluR5 expressions were detected. Oxygen and glucose deprivation/reoxygenation (OGD/R) was performed on primary astrocytes (ASTs) to induce cell swelling. MB was administered at the beginning of reoxygenation, and the perimeter of ASTs was measured by GFAP immunofluorescent staining. 3,5-dihydroxyphenylglycine (DHPG) and fenobam were given at 24 h before OGD to examine their effects on MB functions on AST swelling and AQP4 expression. MB remarkably decreased the volumes of T2WI and ADC lesions, as well as the cerebral swelling. Consistently, MB treatment significantly decreased GFAP, mGluR5 and AQP4 expression at 48 h after stroke. In the cultivated primary ASTs, OGD/R and DHPG significantly increased ASTs volume as well as AQP4 expression, which was reversed by MB and fenobam treatment. The obtained results highlight that MB decreases the post-ischemic brain swelling by regulating the activation of AQP4 and mGluR5, suggesting potential applications of MB on clinical ischemic stroke treatment.

1. Introduction

Brain edema has been recognized as a consequence of fluid accumulation inside brain cells as well as extracellular spacing. This

* Corresponding author. Department of Cardiovascular, The Traditional Chinese Medicine Hospital of Shijiazhuang, No.233, Zhongshan West Road, Qiaoxi District, Shijiazhuang, 050011, Hebei, China.
E-mail address: 15200019815@163.com (Y. Lai).
[1] Yu Lai and Jie Han contributed equally to this work and share first authorship.

https://doi.org/10.1016/j.heliyon.2024.e29483
Received 11 October 2023; Received in revised form 7 April 2024; Accepted 8 April 2024
Available online 12 April 2024

may be one of the common complications related to various central nervous system (CNS) diseases, such as ischemic stroke, brain injury, cerebral aneurysm rupture, inflammation and brain tumors [1]. The hazards of brain edema include the reduced brain blood flow, elevated intracranial pressure, cerebral palsy or even death. The treatments for brain edema include decompressive craniectomy and osmotic therapy, which are only used to control the end-stage events but not directly inhibit the underlying molecular mechanisms of brain edema.

Aquaporins (AQPs) are a specific type of aquaporin family, and the first aquaporin was discovered in 1991 [2]. AQP4 is the most abundant AQPs in the brain and is mainly expressed in the end foot of astrocytes (ASTs), at synapses, and at the glia limitans [3]. Studies have demonstrated changes in the expression of AQP4 in some brain disease such as cerebral ischemia, brain tumors, subarachnoid hemorrhage and other diseases [4]. Various studies have also shown that AQP4 can mediate water exchange across the blood–spinal cord and blood–brain barriers (BSCB/BBB), and controls cell volume, extracellular space volume, and astrocyte migration. It participate in regulating water molecules in a doubled-way manner, which are promoting cytotoxic brain edema, and eliminating vasogenic brain edema [5].

A large amount of excitatory amino acids, such as glutamate, are released after cerebral ischemia [6]. Glutamate mainly acts in the brain through glutamate receptors. Glutamate receptors are categorized into 2 types, namely, metabotropic and ionotropic glutamate receptors (mGluRs and iGluRs, respectively). Pharmacological and biological experiments have shown that both mGluRs and iGluRs exist in AST, and metabotropic glutamate receptor 5 (mGluR5) is the main mGluRs receptor subtype in CNS [7]. Recent studies have shown that the Homer1-mGluR5 and downstream mammalian target of rapamycin (mTOR) signaling pathways were closely related the pathophysiology of depression [8]. mGluR5 of AST plays an important role in glial-neuron interactions, thereby regulating the reuptake of glutamate and modulating neuronal activity coupled with neurovascular units [9]. The activation of mGluRs has been found to result in astrocyte (AST) swelling. The mechanisms regarding the effect of mGluR5 activation on AQP4 expression appear to be complex [10]. It has been reported that mGluR5 can initiate calcium release from intracellular stores, which promotes the activation of Ca^{2+} signaling pathways [11]. In addition, Ca^{2+} has been shown to be a major trigger for AST swelling and AQP4 activation following traumatic brain injuries (TBI) and stroke, which can be mediated through the transient receptor potential (TRP) channels and the endocytosis pathways [12]. A previous study by Ref. [13] reported that glutamate could activate mGluR5 expression and further lead to activation of calcium/calmodulin-dependent protein kinase II (CaMKII) and nitric oxide synthase (NOS), which targeted the AQP4 serine 111 residue and induced AST swelling.

In 1876, methylene blue (MB) which is a blue textile dye was initially prepared and it was utilized to treat cyanide poisoning, methemoglobinemia and malaria [14]. Recent studies have demonstrated the potential neuroprotective properties of MB in the treatment of Parkinson's disease (PD) and ischemic stroke models [15]. MB was found to reduce cerebral ischemia reperfusion damage in a transient focal cerebral ischemia model by rerouting mitochondrial electron transfer and increasing mitochondrial oxidative phosphorylation [16]. Previous studies have shown the involvement of various elements of MAPK/ERK/JNK pathways in CNS disorders using primary human ASTs [17,18]. A recent study demonstrated that MB could improve brain edema and AST swelling by the inhibition of AQP4 expression via the ERK1/2 pathway [19].

Although the protective effect of MB on brain edema has been confirmed [20], the protective mechanism of MB on postischemic brain edema remains unclear. Therefore, through using the transient middle cerebral artery occlusion (tMCAO) approach, a rat model of brain edema induced by brain ischemia/reperfusion injury was created to assess the therapeutic effects of MB on brain edema. The magnetic resonance imaging (MRI) was used to assess the therapeutic effect of MB. The AST swelling was assessed by the morphological observation and cell perimeter measurement according to the glial fibrillary acidic protein (GFAP) staining. Further the study investigated the impact of AQP4 and mGluR5 on MB in the treatment of brain edema, clarified the mechanism of MB treatment against brain edema, and provided the necessary theoretical and experimental basis for the further application of MB.

2. Materials and methods

2.1. Animals and management

The study protocol received approval from the Animal Care and Use Committee at Beijing Neurosurgical Institute (No.

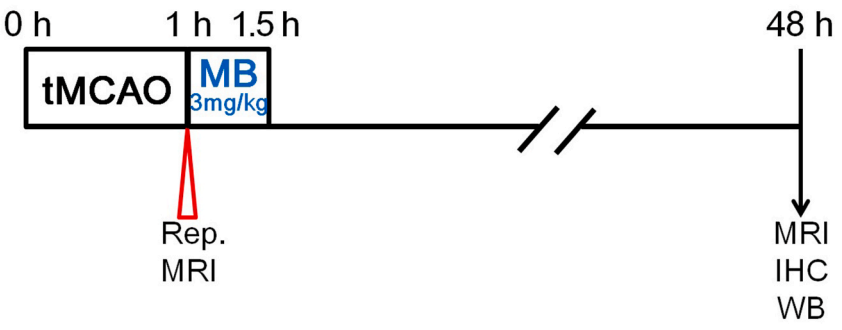

Fig. 1. Experimental design schematic diagram.

201401007). The current study was carried out at Beijing Neurosurgical Institute. Animal intervention procedure was performed according to the Guidelines for the Care and Use of Laboratory Animals. Fifty-two Sprague–Dawley (SD) male rats of 220–250 g were provided by Vital River Laboratories (Beijing, China). The animals were raised for 7 days for acclimatization within polypropylene cages under controllable laboratory conditions and were allowed to drink water and eat food freely.

2.2. Experimental design and procedure

Rats were randomly assigned into 3 groups: the sham operation (control) group (n = 12), transient middle cerebral artery occlusion (tMCAO) with vehicle and tMCAO with MB treatment groups (n = 20 in each group). In the MB treatment group, rats were intravenously injected with MB (Cat.#M9140, Sigma Aldrich, St. Louis, MO) via the tail vein (3 mg/kg, 4 mL kg^{-1} h^{-1}, ~30 min) following reperfusion. The tMCAO and vehicle treatment group was given an intravenous injection of an equivalent volume of normal saline. Fig. 1 shows the experimental procedure. Six animals died due to subarachnoid hemorrhage (4 in the tMCAO + vehicle group and 2 in the tMCAO + MB group), which was therefore eliminated from subsequent analyses.

2.3. Transient middle cerebral artery occlusion

Transient middle cerebral artery occlusion (tMCAO) was induced according to previous descriptions in Ref. [21]. In brief, each rat was given an intraperitoneal injection of a xylazine/ketamine mixture dissolved in normal saline (10 and 100 mg/kg, respectively) for anesthesia. In addition, the body temperature (measured rectal) was kept under 37 °C during the whole surgical process by the thermally controlled operating table as well as the heating blanket. Afterwards, the left internal carotid artery, external carotid artery, and common carotid artery were exposed through one midline incision under the operation microscope. Then, a filament that was 0.38 mm in diameter and coated with silicon was pushed forwards from the external carotid arterial lumen to the internal carotid artery until resistance was felt to ensure that the middle cerebral arterial origin was occluded. Then, the filament was maintained in situ for 1 h before it was retracted gently for ischemic territory reperfusion. The identical surgical process was carried out in the Sham rats, except for the insertion of the filament.

2.4. Magnetic resonance imaging (MRI)

Sixteen rats (8 from the tMCAO + MB group and 8 from the tMCAO + vehicle group) were subjected to sequential MRI 48 h after occlusion using 7.0 T scanner (BioSpec, Bruker, Billerica, Germany) that was equipped with a four-channel phased array thread coil. Diffusion-weighted images (DWI) were obtained by the spin–echo echo-planar imaging sequence according to the following parameters: matrix of 128 × 108, field of view (FOV) of 4 × 4 cm, b-value of 1000 s/mm^2, repetition time (TR) of 4500 ms, slice thickness (THK) of 1 mm, number of averages (NA) of 1, and echo time (TE) of 35 ms.

Quantitative maps of the apparent diffusion coefficient (ADC) were computed on the basis of 2 distinct b-values (namely, 0 and 1000 s/mm2). Then, the T2-weighted turbo-spin echo images (T2WI) were obtained through the fast spin–echo sequence (matrix of 320 × 240, FOV of 4 × 4 cm, NS of 20, THK of 1 mm, NA of 1, TE of 37 ms, and TR of 3140 ms). Afterwards, OsiriX software was used to analyze the images.

To quantify the lesion size on both ADC and T2WI images, the brain lesion areas within each slice were depicted via two investigators. The region of interest (ROI) was defined by the operator on every slice containing the lesion. Then the lesion volume as well as brain region in every rat was determined. Later, an identical method was used to measure the brain area on the contralateral side based on previous study by Ref. [20].

Hyperintense pixels on T2WI, together with hypointense pixels on ADC within the ipsilateral cortex were defined as lesion area for calculation and statistics. Thus, the volume of the lesion displayed on ADC and T2WI (Vu) was measured as the sum of hypointense or hyperintense areas within every slice multiplied by the thickness of the slice. To further offset the brain edema presence, the corrected volume of the lesion (Ve %) together with the brain edema %, which were presented in the form of an increase in the affected hemisphere volume were computed by the equation below described by Ref. [22]:

$$Ve = Vc + Vi - (Vc + Vi - Vu)\frac{Vc + Vi}{2Vc}$$

$$\text{Swelling } \% = \frac{2(Ve - Vu)}{Vc + Vi} \bullet 100$$

in which Vu and Ve represent the uncorrected and corrected volumes of the lesion, respectively, whereas Vc and Vi represent the contralateral and ischemic hemisphere volumes, respectively.

2.5. Staining with 2,3,5-triphenyltetrazolium chloride (TTC)

To determine the eventual lesion volume, TTC staining was carried out on 8 rats from the tMCAO + MB group and 8 rats from tMCAO + vehicle group at 48 h after occlusion. All animals were then subjected to re-anesthesia, followed by sacrifice through decapitation for collecting the whole brain tissues. Then, the brain tissues were sliced into coronal sections that were 2 mm in thickness, followed by 15 min of incubation with 2 % TTC solution (Cat.#T8877, Sigma Chemical, St. Louis, MO), and finally subjected

to 24 h fixation within 4 % formaldehyde. ImageJ (NIH, Bethesda, Maryland) software was used to analyze the infarction volume. Meanwhile, the equation below was used to calculate the infarct volume percentage (Infarct %):

$$\text{Infarct } \% = \frac{\text{Vc} - \text{Vl}}{\text{Vc}} \bullet 100$$

where Vc represents contralateral hemisphere volume, while Vl stands for non-ischemic tissue volume within the affected hemisphere.

Brain edema (swelling %) was also calculated according to the following formula:

$$\text{Swelling } \% = \frac{\text{Vi} - \text{Vc}}{\text{Vc}} \bullet 100$$

in which Vi indicates the ischemic hemisphere volume.

2.6. Hematoxylin and eosin (HE) staining and immunohistochemistry (IHC) analysis

Rats were subjected to re-anesthesia after 48 h of occlusion. Then rats received transcardial perfusion with saline, then with 4 % paraformaldehyde. Brain tissues were harvested and postfixed in 4 % paraformaldehyde at 4 °C for 24 h, followed by dehydrated, wax immersion, paraffin embedding, and slicing into sections (4 μm). Following deparaffinization and hydration, HE staining was carried out.

For the IHC assay, each section was subjected to blocking with 5 % bovine serum albumin (BSA) following antigen retrieval. Then incubation at 4 °C overnight with the primary antibody, rabbit anti-rat AQP4 (Cat.# ab128906, 1:200, Abcam, MA, USA) or rabbit anti-rat GFAP (Cat.#Z0334, 1:500, DAKO, Glostrup, Denmark). Afterwards, the antigen–antibody complexes in each section were detected by an EnVision Detection Kit (Cat.#K5007, DAKO). A microscope (Carl Zeiss, Oberkochen, Germany) was used to photograph the HE and IHC staining at the ischemic penumbra of cortical regions for each section. The mean of optical density was calculated using ImageJ (NIH, Bethesda, Maryland). Three fields of the IHC images in the ischemic penumbra of cortical regions from 5 rats in each group were randomly selected to calculate the mean optical density.

2.7. Astrocytes cell culture

Cortical ASTs were cultured in accordance with the protocol described by Ref. [23] after mild modification. In brief, rats of one day age were subjected to ether anesthesia, followed by sterilization with 75 % alcohol. Afterwards, the brain was extracted from the skull, followed by careful stripping of the meninges. The brain tissue was subsequently minced and resuspended, followed by dissociation into singular cells under gentle pipetting. Thereafter, the cells were collected, filtered with a 74-μm Nitex mesh and cultured in Minimum Essential Medium (MEM) containing 10 % fetal bovine serum (FBS) in air containing 5 % CO_2 at 37 °C. Typically, the culture medium was changed at an interval of 3–4 days. Then, subculture was conducted 10 days after primary culture to acquire a larger number of ASTs, and the ASTs of the second passage were utilized for each experiment. Primary ASTs are very sensitive to contaminations such as mycoplasma, and the cell status are monitored to ensure that the cells are in good condition before carrying out each experiment and to ensure the reproducibility of the experiments.

2.8. Oxygen and glucose deprivation/reoxygenation (OGD/R) procedure and drug treatment

Twenty-four h prior to OGD, 100 μM (S)-3,5-dihydroxyphenylglycine (DHPG, selective mGluR5 agonist, Cat.# 0805, TOCRIS, Bristol, UK) and 300 μM fenobam (selective mGlu5 antagonist, Cat.# 2386, TOCRIS) were administered to examine their effects on AST swelling and AQP4 expression. For OGD, all cells were first rinsed with sterile PBS twice, followed by 6 h of incubation in DMEM depleted of FBS, pyruvate and glucose (Thermo Scientific) in an anaerobic chamber containing 5 % CO_2 and 0.1 % O_2 at 37 °C. Upon OGD completion, all the cell cultures were washed once, followed by 48 h of incubation under normal conditions (reoxygenation). During reoxygenation (Reox), AST cultures were treated with MB at various concentrations (0.01–10 μM).

2.9. Quantification and immunocytochemistry

ASTs that were cultivated onto glass coverslips to reach the confluency of about 50%–60 % and were subjected to 10 min of acetone fixation, 20 min of blocking using goat serum contained in PBS, and overnight incubation using rabbit anti-rat AQP4 (Cat.# ab128906, 1:50, Abcam) and rabbit anti-rat GFAP (Cat.#Z0334, 1:75, DAKO) antibodies at 4 °C. The next day, the cells were subjected to 1 h of incubation with Alexa Fluor 488-conjugated goat anti-rabbit IgG (H + L) antibody (Cat.# A-11008, 1:200, Life Technologies, CA, USA) at room temperature. Finally, the cells were observed and photographed using an inverted fluorescence microscope (Carl Zeiss). The primary antibody was replaced with PBS in the negative control group.

2.10. Immunofluorescent staining for AQP4 and mGluR5 in brain tissues

Immunofluorescence staining for mGluR5 and AQP4 was also performed on brain sections. Sections (4 μm) were blocked in 5 % bovine serum albumin and then subjected to overnight incubation using the anti-AQP4 (Cat.# ab128906, 1:100, Abcam) rabbit

polyclonal antibody as well as the anti-mGluR5 (Cat.# ab76316, 1:200, Abcam) mouse polyclonal antibody at 4 °C and then 1 h of secondary antibody incubation (TRITC/Alexa Fluor 488-labelled anti-rabbit/mouse IgG) at ambient temperature. Sections were washed with PBS before being mounted with DAPI fluorescent mounting media. Using a fluorescence microscope (Carl Zeiss), the sections were photographed.

2.11. Cell perimeter measurement

The perimeter of ASTs was utilized to represent the volume of ASTs as described by our previous study [11]. Following GFAP immunofluorescence staining, the perimeter values were computed by Image-Pro Plus software (Media Cybernetics, Rockville, MD, USA). Afterwards, three fields were selected from three wells for measurement in each group, the nine fields were averaged to determine the perimeter of the cell in every group. Ten cells were selected randomly from every field under a microscope at a high magnification of 200 × .

2.12. Western blotting assay

Western blotting was performed to determine AQP4 protein expression. ASTs were subjected to 10 min of 0.25 % trypsin digestion under ambient temperature before they were harvested using the cell scraper. Afterwards, the collected ASTs were subjected to on-ice cell lysis buffer, followed by cell disruption using an ultrasonic machine.

The BCA approach was adopted to determine the protein content. Then, the protein samples were subjected to 15 min of denaturation at 85 °C and separation through 10 % sodium dodecyl sulfate–polyacrylamide gel electrophoresis (SDS–PAGE), followed by 40 min of transfer onto 0.45-mm polyvinylidene fluoride (PVDF) membranes under a voltage of 22 V. Later, 5 % skimmed milk contained within Tris-saline buffer (TBS) was used to block the nonspecific binding sites at ambient temperature for 2 h. Afterwards, anti-AQP4 polyclonal antibodies (Cat.# ab46182, 1:500, rabbit anti-rat, Millipore, Abcam, MA, USA) were used to incubate the PVDF membranes at 4 °C overnight, followed by 1 h of incubation with secondary antibody (horseradish peroxidase (HRP)-conjugated goat anti-rabbit IgG, diluted at 1:1000, Cell Signaling Technology, Danvers, MA, USA) at ambient temperature. Then, an enhanced chemiluminescence reagent kit was adopted to detect specific bands in accordance with the manufacturer's protocols. Mouse anti-rat β-actin (Cat.# A5441, 1:5000, Sigma, St. Louis, MO, USA) served as an internal reference. ChemiDoc MP (Bio-Rad) was used to analyze the bands. The findings were obtained on the basis of 3 repeated independent samples which were repeated for 3 times.

2.13. Statistical analysis

Statistical analyses were performed using Prism software package (version 8.2.1). Differences between the vehicle and MB treatment groups were determined through the independent *t*-test. One-way analysis of variance (ANOVA) tests followed by post hoc Tukey's test were used to compare between multiple groups when data was normally distributed. A p value of <0.05 was considered statistically significant. Results were expressed as mean ± standard deviation (SD).

3. Results

3.1. Volume of lesions displayed on T2WI and ADC

First, rats underwent MRI testing prior to MB treatment (before reperfusion) to determine the lesion volume. The ischemia lesions

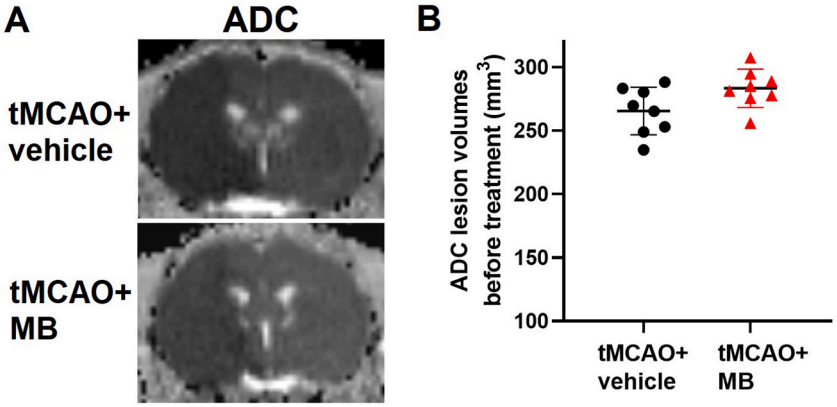

Fig. 2. MRI testing was performed prior to MB treatment (before reperfusion) to determine the lesion volume. (A). ADC images of rats in tMCAO + vehicle and tMCAO + MB groups prior to MB treatment (before reperfusion) to ensure the lesion volumes. (B). Quantitative analyses on the ADC lesions in vehicle and MB treatment groups before reperfusion.

on ADC were limited to the middle cerebral artery boundary, which included the frontoparietal cortex and basal ganglia. ADC lesions showed no significant difference between the MB treatment and vehicle treatment groups, and they were 265.3 ± 18.73 and 285.0 ± 15.13 mm^3, respectively ($p > 0.05$, Fig. 2A-B). No lesions could be observed in the sham-operated rats.

Moreover, at 48 h after occlusion, rats received MR examination again to test the MB treatment effect. The lesion on ADC was enlarged compared with that before reperfusion, accompanied by the lesion on T2WI. After 48 h of tMCAO, the eventual lesion volume on ADC reached 206.5 ± 16.58 and 311.3 ± 15.01 mm^3 in the MB treatment and vehicle treatment groups, respectively ($p < 0.001$, Fig. 3A-B). In addition, the corrected lesion volume on T2WI reached 22.75 ± 1.23 % and 31.34 ± 2.59 % in the MB and vehicle groups, respectively ($p < 0.01$, Fig. 3C). In addition, MB treatment (15.53 ± 1.04 %) markedly reduced ischemia-related brain edema relative to that in the vehicle group (20.53 ± 1.37 %) ($p < 0.01$, Fig. 3D).

At 48 h following tMCAO, TTC staining indicated that the volume of infarct lesions was 31.5 ± 1.01 % and 37.64 ± 0.85 % in the MB and vehicle groups, respectively (Fig. 4A-B, $p < 0.05$). Consistent with the T2WI results, TTC staining results also showed that treatment with MB dramatically ameliorated ischemia-related brain edema, which was 10.14 ± 0.70 % and 15.39 ± 0.86 % in the MB and vehicle groups, respectively ($p < 0.05$) (Fig. 4C).

3.2. OGD/R-induced astrocyte swelling

Brain edema and AST swelling was evaluated both *in vitro* and *in vivo*. As shown in Fig. 5A, HE staining revealed that neurons were regularly arranged, and capillary morphogenesis and glial cells showed no abnormalities in the sham group. Following tMCAO, a majority of cells showed disordered arrangement, and severely shrunken or pyknotic nuclei, together with cellular swelling and hypervacuolization, were observed in certain areas, which was ameliorated by MB treatment.

Fig. 5B showed that the expression of GFAP, the marker of ASTs, was increased in the tMCAO group, which was ameliorated by MB treatment. Furthermore, AQP4 protein expression, mainly located in the endfeet of ASTs and around the blood vessels, was upregulated following tMCAO, which was inhibited by MB treatment.

Moreover, primary ASTs were cultured and subjected to 6 h OGD plus 48 h Reox injuries. Immunofluorescence staining further revealed that AST volume was significantly increased by OGD/R injury but was decreased by MB treatment (Fig. 6). According to Western blotting, after 48 h of reoxygenation injury, AQP4 protein expression was increased (0.077 ± 0.009, $P < 0.05$) in comparison with that in the control group (0.023 ± 0.001), and this result consistent with the results of immunofluorescence staining of AQP4 (Fig. 7A-B). Additionally, acute treatment with 10 μM MB after OGD significantly reduced the AQP4 expression induced by OGD/R (0.052 ± 0.005, $P < 0.05$) (Fig. 7B).

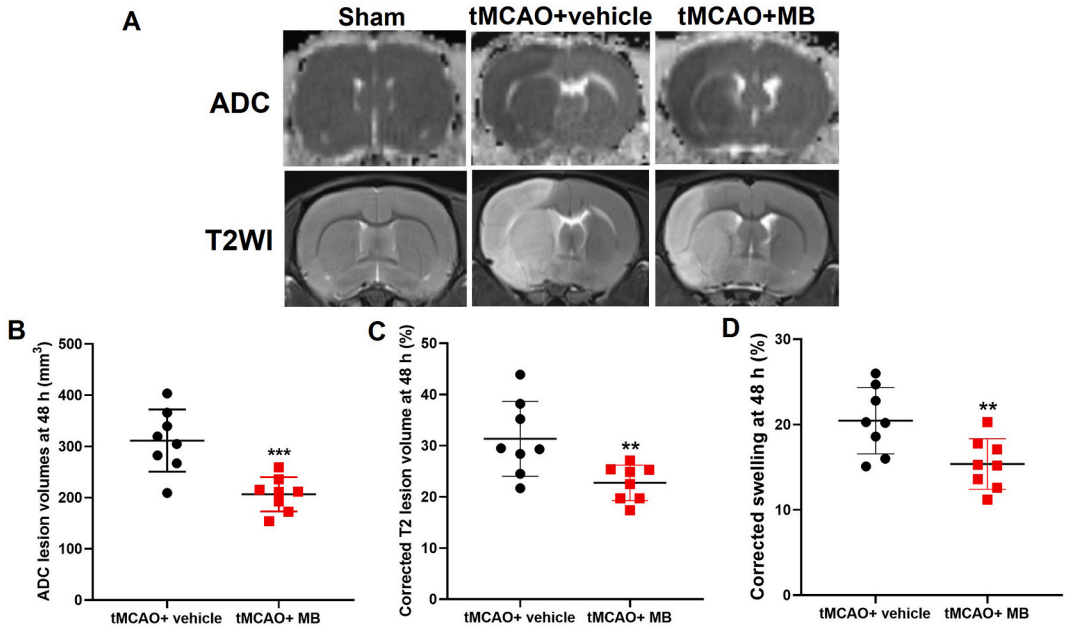

Fig. 3. Effect of MB on brain edema resulting from focal transient brain ischemia. (A). ADC and T2WI images for the MB- and vehicle-treated rats at 48 h following tMCAO. (B). ADC evolution defines the volumes of ischemia lesions in MB and vehicle treatment groups at 48 h. (C). Quantitative analyses of the corrected lesion volume on T2WI in the MB and vehicle treatment groups at 48 h following tMCAO. (D). Quantitative analyses of brain edema predicted with T2WI images at 48 h following tMCAO. All values are shown as the mean ± SD, $^{**}p < 0.01$, $^{***}p < 0.001$ vs. tMCAO + vehicle group.

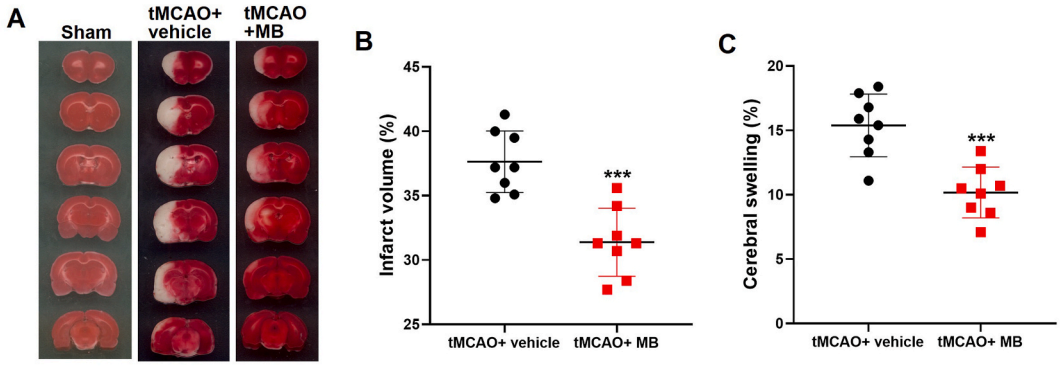

Fig. 4. Effect of MB on transient brain ischemia induced brain infarction and edema was evaluated using TTC staining. (A). Typical TTC staining for cerebral sections in MB and vehicle treatment groups at 48 h after tMCAO. (B) Quantitative analyses of the lesion volumes defined by TTC in MB- and vehicle-treated rats. (C) Quantitative analyses of TTC staining in MB- and vehicle-treated rats. All values are shown as the mean ± SD, ***p < 0.001 vs. tMCAO + vehicle group.

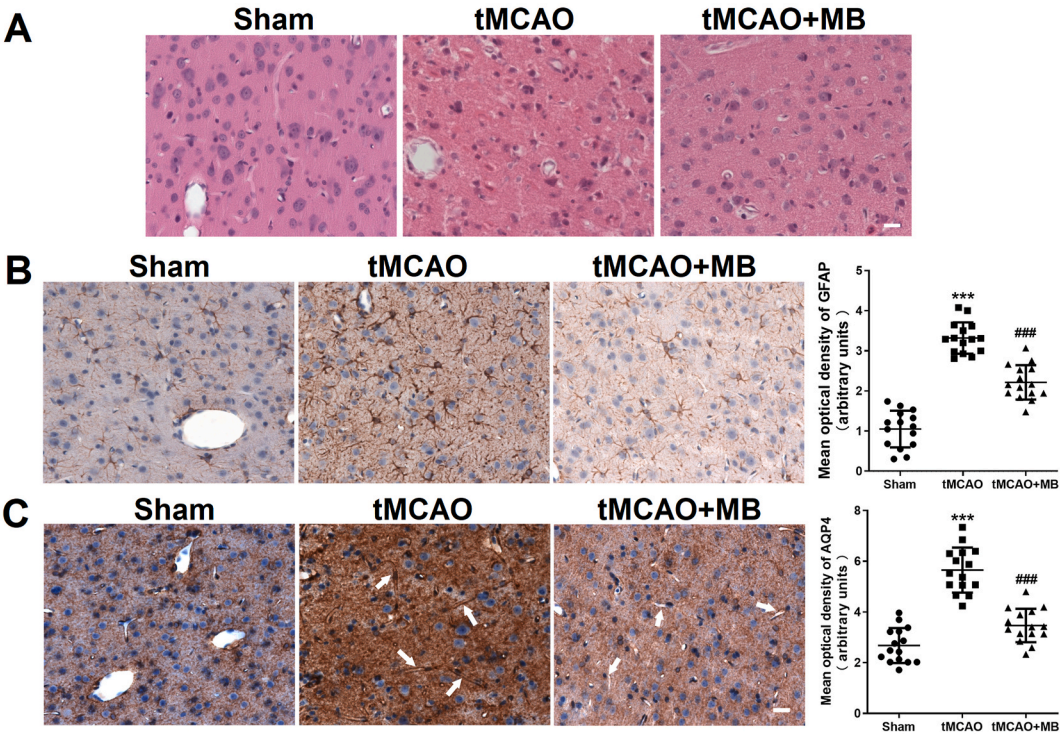

Fig. 5. Effect of MB on the GFAP and AQP4 expression in tMCAO rats. (A). HE staining images showing neuropathological changes in each group. (B). IHC staining and quantitative analysis showing AQP4 and GFAP expression at the ischemic penumbra of cortical regions. AQP4 expression around blood vessels was indicated by white arrows. Scale bars show 20 μm. Three fields of the IHC images in the ischemic penumbra of cortical regions from 5 rats in each group were randomly selected to calculate the mean optical density. All values are shown as the mean ± SD, ###p < 0.001 vs. tMCAO group, ***p < 0.001 vs. sham group.

3.3. AQP4 and mGluR5 expression within tMCAO brain tissue

The effect of MB on mGluR5 and AQP4 expression was examined after brain edema within both cultivated ASTs and the tMCAO rat model. Immunofluorescence double staining of AQP4 and mGluR5 was first performed and results showed the co-expression of AQP4 and mGluR5 in cultured ASTs (Fig. 8A). Meanwhile, GFAP and AQP4 double immunofluorescence staining in the brain tissues of each group showed that AQP4 in ASTs was increased after tMCAO (Fig. 8B), which was consisted with the study from our group [24].

According to quantitative analysis, AQP4 and mGluR5 expression was increased in the tMCAO group (1.041 ± 0.1180) relative to the sham group (0.7537 ± 0.0445; Fig. 9A) but decreased in the MB group (0.8606 ± 0.04119). The expression of mGluR5 and AQP4

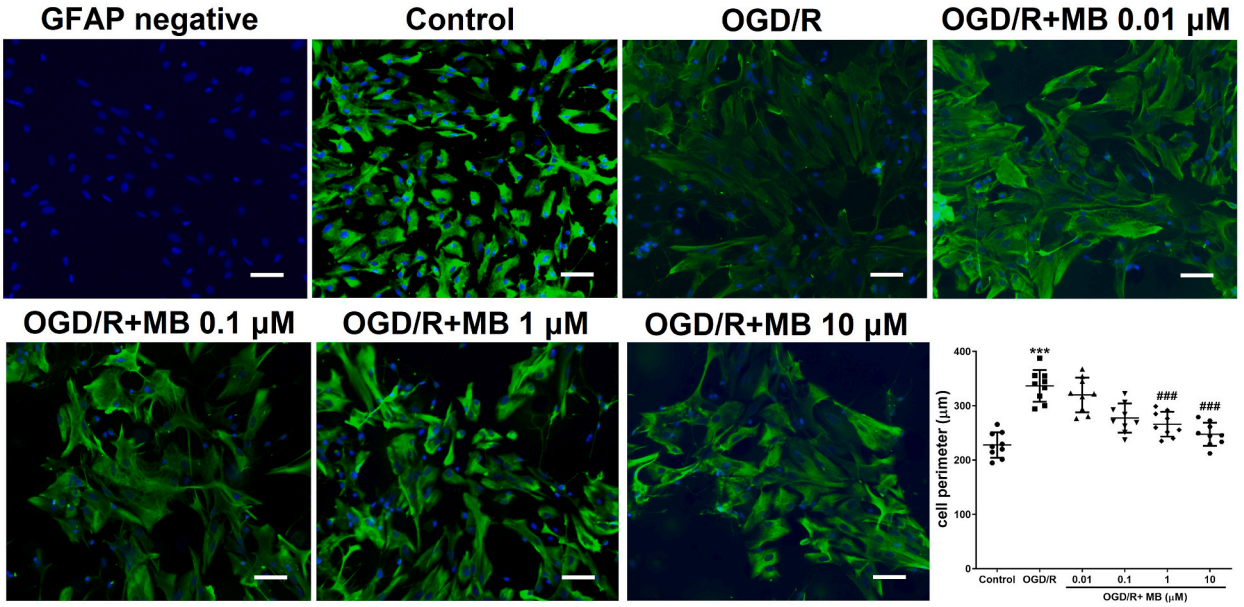

Fig. 6. Effect of MB on astrocyte swelling induced by OGD/R. Astrocytes were injured by OGD/R and treated with different concentrations of MB (0.01–10 μM). Immunofluorescence staining for GFAP in cultured astrocytes. Scale bars show 50 μm. Quantitative analyses of the image data obtained based on the panels within (A) revealed the astrocyte perimeters in each group. Ten cells in each field under high magnification (200 ×) were randomly selected. Three fields in three wells were measured in every group, and the values of nine fields were calculated as the cell perimeter of each group. Values are displayed as the mean ± SD. ###p < 0.001 vs. OGD/R group, ***p < 0.001 vs. Control.

was rarely detected within normal cerebral tissues and was upregulated following tMCAO (Fig. 9B) and downregulated in the MB treatment group relative to the tMCAO group. Increased AQP4 and mGluR5 expression was also detected within the AST membrane following tMCAO, which was attenuated by MB treatment, suggesting that MB could relieve ischemic cerebral swelling by affecting the expression of mGluR5 and AQP4.

3.4. Effects of MB on the astrocyte swelling and AQP4 expression

DHPG resulted in AST swelling as well as upregulated AQP4 expression, similar to the OGD/R effect (Fig. 10A-B). In addition, MB treatment decreased AQP4 and mGluR5 expression within the cultured ASTs with OGD/R and DHPG treatment (Fig. 10C-D). In addition, similar to MB effects, as a selective mGluR5 antagonist, the administration of fenobam also reversed OGD/R and DHPG-derived AST swelling as well as decreased AQP4 expression within cultivated ASTs. These results indicated that the effect of MB on AST swelling and AQP4 expression was directly dependent on mGluR5 functions.

4. Discussion

Brain edema, which is a severe consequence of ischemic stroke, is a complex and catastrophic neurological disease with few effective treatments available. In this study, the effect of MB on brain edema in both tMCAO rats and cultured ASTs was investigated. It was found that relative to vehicle-treated rats, the infarction and edema percentage in the MB group were decreased 48 h after tMCAO. MB inhibited the upregulation of AQP4 and mGluR5 in the ischemic peripheral cortex. Further cellular-level studies have found that MB could attenuate AST edema caused by the mGluR5 agonist DHPG and simultaneously reduce the expression of AQP4, indicating that the effect of MB on AST swelling and AQP4 expression was directly dependent on mGluR5 activation.

Previous studies have shown the ameliorative effect of MB on CNS diseases [15]. Daily oral delivery of low-dose MB could ameliorate olfactory dysfunction and motor deficits in a chronic MPTP/Probenecid mouse model of PD [25]. In an Alzheimer's disease (AD) transgenic mouse model (APP/PS1), MB treatment rescued social behavior, alleviated cognitive deficits and reduced beta-amyloid load in the hippocampus and cortex by restoring the concentrations of alanine and lactate in the brains of transgenic mice [26]. Another study summarized that the mechanisms of MB in AD were mainly related to preventing mitochondrial dysfunction, attenuating energy hypometabolism and preventing the formation of toxic forms of amyloid-β (Aβ) [27]. In addition, studies have also shown that the neuroprotective effect of MB against neuronal OGD/R injuries is regulated by hypoxia-inducible factor-1α (HIF-1α) stabilization and macroautophagy by activation of AMPK signaling [28]. The current results also provided evidence regarding the neuroprotective effect of MB in an ischemic stroke model and showed that MB could ameliorate tMCAO-induced brain edema by regulating mGluR5 and AQP4 expression.

AQP4, an intrinsic membrane protein, is essential for regulating the water balance in the neurological system and, when it is

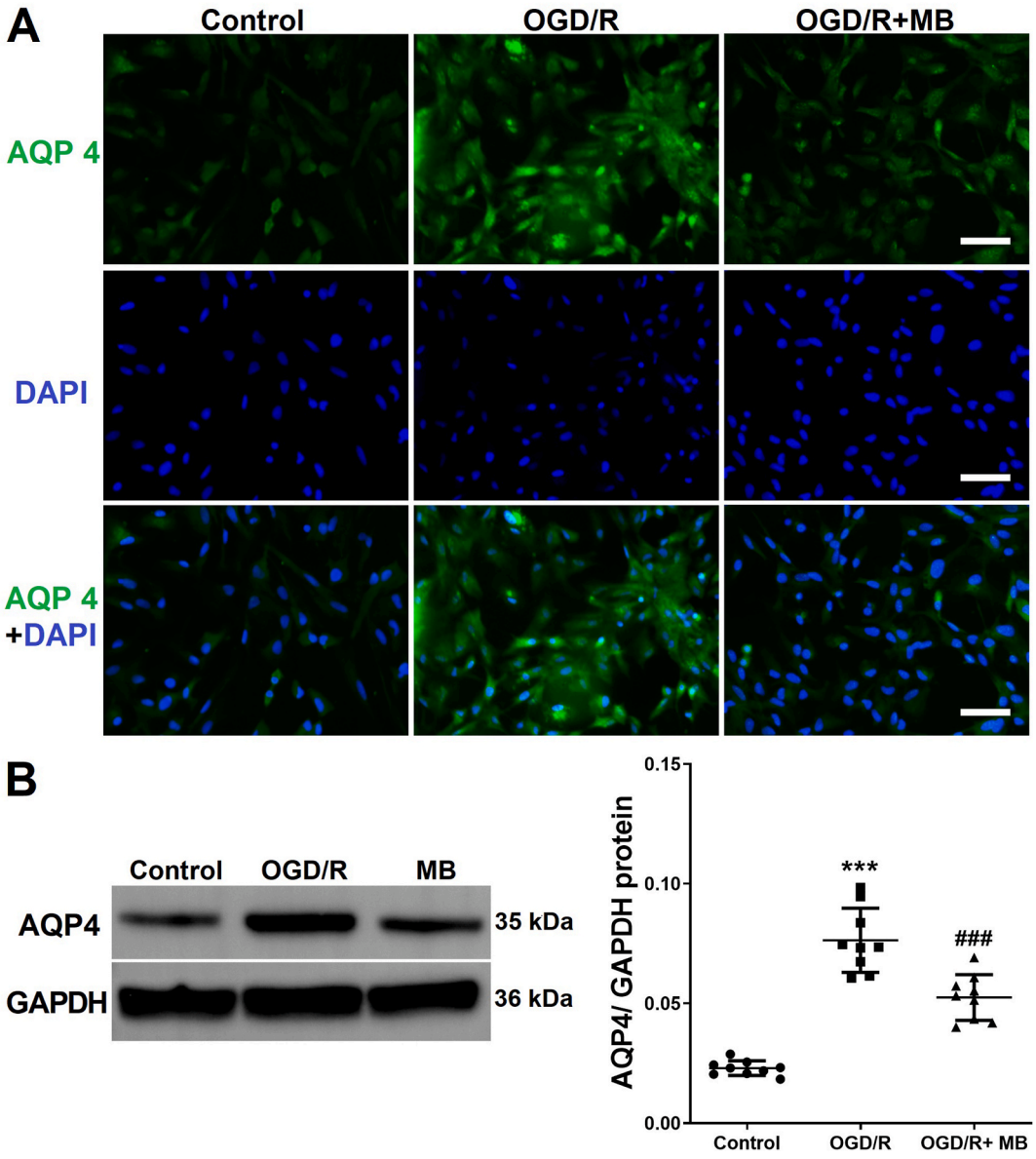

Fig. 7. Effect of MB (10 μM) treatment on AQP4 expression in cultured astrocytes. (A). immunofluorescence staining for AQP4 in cultured astrocytes. Scale bars show 50 μm. (B). Protein expression of AQP4 determined by Western blot and quantitative data. All results are obtained on the basis of 3 repeated independent samples which were repeated for 3 times. Values are displayed as the mean ± SD. ###$p < 0.001$ vs. OGD/R group, ***$p < 0.001$ vs. Control.

dysfunctional, can result in brain edema [29]. AQP4 protein is abundantly expressed in ASTs of the blood–brain barrier and cerebrospinal fluid-brain membrane, mediating water movement between fluid cavities (blood and cerebrospinal fluid) and the brain parenchyma [5]. In water toxicity and focal cerebral ischemia models, studies have shown that AQP4 deficiency significantly reduces cytotoxic brain edema [30]. Changes in AQP4 expression were observed during brain edema caused by TBI, degenerative diseases, brain tumors, ischemia, epilepsy, and other neurological diseases [5,31,32]. A study from Kitchen et al. demonstrates that CNS edema is associated with increases both in total AQP4 expression and AQP4 subcellular translocation to the blood-spinal-cord-barrier (BSCB). Pharmacological inhibition of AQP4 translocation to the BSCB prevents the development of CNS edema and promotes functional recovery in injured rats [33]. This role has been confirmed by the Sylvain et al. which has demonstrated that targeting AQP4 effectively reduces cerebral edema during the early acute phase in the photothrombotic stroke model. They have also shown a link to brain energy metabolism as indicated by the increase of glycogen levels [34]. After tMCAO treatment, AQP4-deficient mice show better neurological and functional outcomes than normal control mice, and the brain edema severity in AQP4-deficient mice is 35 % lower than that in normal control mice 24 h after injury [35]. However, in the subarachnoid hemorrhage model, the severity of brain edema of

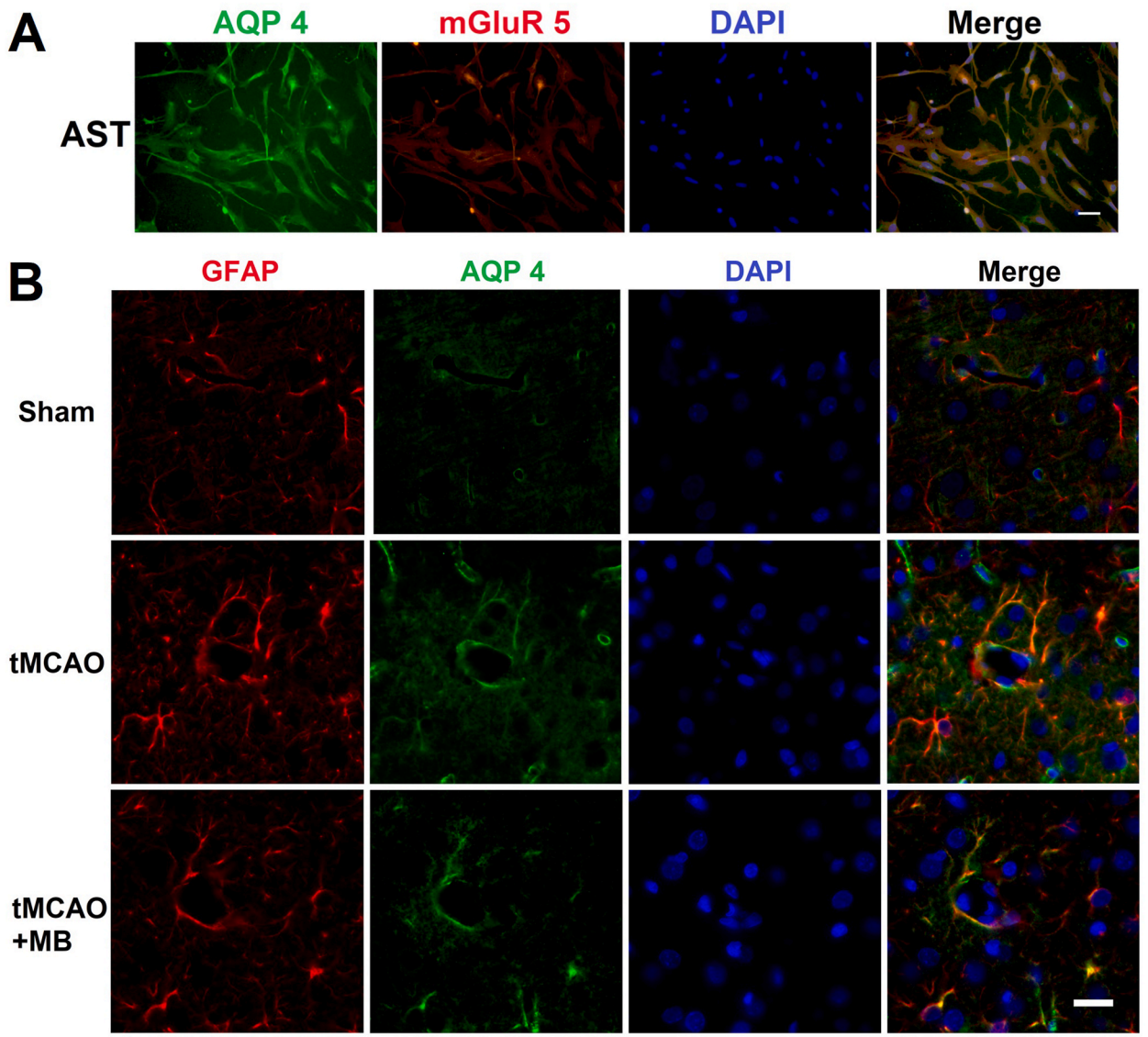

Fig. 8. Co-expression of AQP4 and mGluR5 in astrocytes. (A) Immunofluorescence double staining of AQP4 and mGluR5 in cultured astrocytes. (B) GFAP and AQP4 double immunofluorescence staining in the brain tissues of each group. Scale bars show 20 μm.

AQP4-deficient mice is significantly higher than that of normal mice, probably due to the excessive water transport caused by the loss of AQP4 [36]. The different roles of AQP4 in brain edema may be related to the reason and formation time as well as different models of cerebral edema. The present study has shown that MB can reduce the expression of AQP4 at the animal and cellular levels, exerting significant therapeutic effects on brain edema.

Some recent indicated that calcein staining fluorescence assay could be used to analyze cell volume on short timescales based on the fluorescence assay [37]. Meanwhile, it could also be used to quantify plasma membrane water permeability in all adherent cell types through real-time monitoring calcein fluorescence quenching [37,38], which is helpful for the future studies on AST functions and AQP4 related mechanisms.

ASTs are increasingly recognized as partaking in complex homeostatic mechanisms critical for regulating neuronal plasticity following CNS insults [39]. Depending on the context and type of injury, reactive astrocytes respond with diverse morphological, proliferative and functional changes collectively known as astrogliosis, which results in both pathogenic and protective effects [40]. There is also growing interest in how astrogliosis might in some contexts be protective and help to limit the spread of the injury. Stroke and TBI are characterized by multiple stages of cerebral edema in the acute and chronic phases following the injury, with most of the initiating mechanisms related to astrocytes [41,42]. Cytotoxic edema is the first stage of cerebral edema in the acute and subacute phases of the brain injuries, which are characterized by distinct pathological mechanisms with oxidative stress, neuroinflammation represented by glial cell activation and cytokine release, and blood–brain barrier (BBB) disruption as key elements that can be targeted

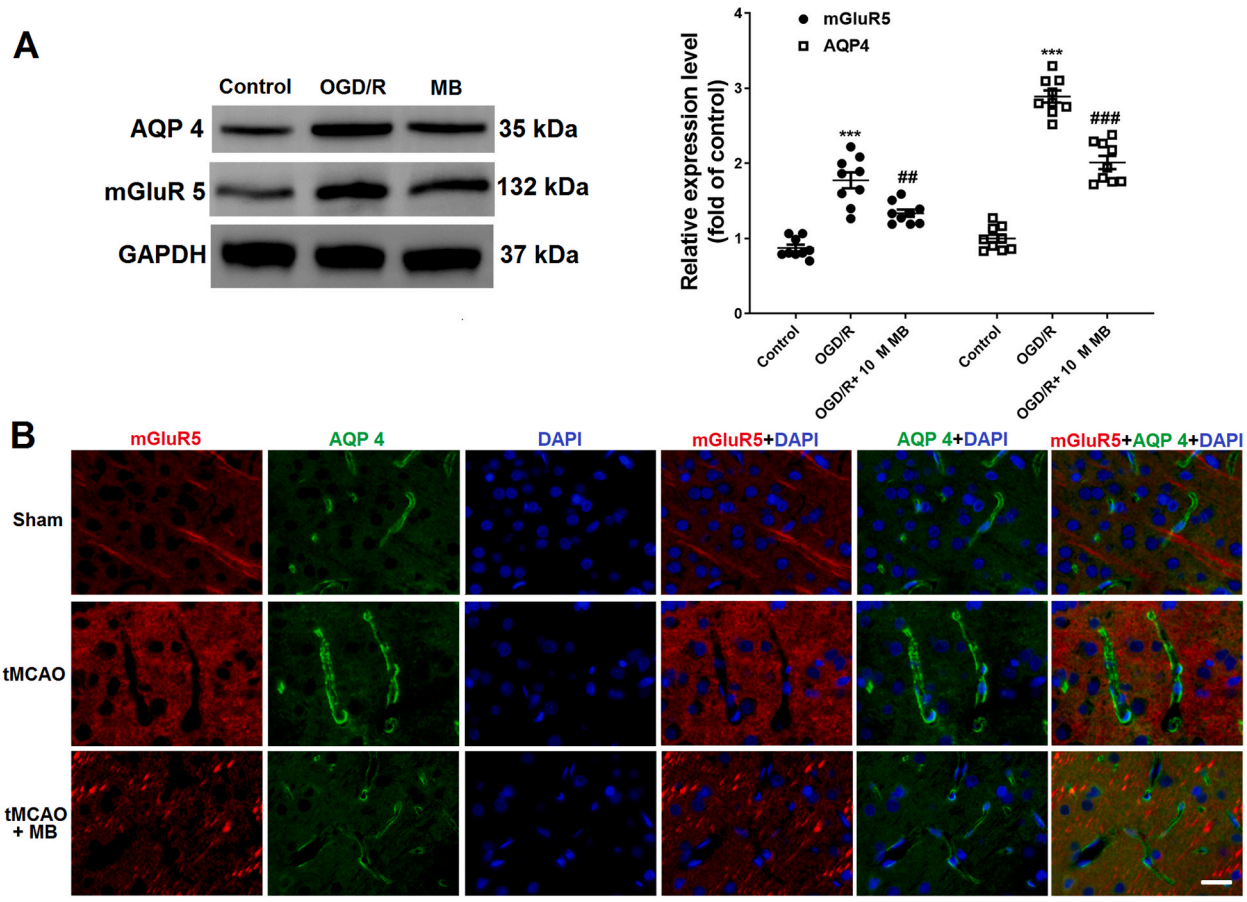

Fig. 9. Effect of MB on the expression of mGluR5 and AQP4 in tMCAO brain tissue. (A). The expression of AQP4 and mGluR5 in cultured astrocytes by Western blotting and its subsequent analysis using ImageJ software (B). Double immunofluorescence staining showing the expression of mGluR5 and AQP4 in pericapillary areas in the normal brain and cell membranes of astrocytes after tMCAO, and MB treatment. Scale bars show 20 μm. All results are obtained on the basis of 3 repeated independent samples which were repeated for 3 times. Values are shown as the mean ± SD, ***$p < 0.001$ vs. control; ##$p < 0.01$, ###$p < 0.001$ vs. OGD/R group.

in this early stage [43,44]. In the chronic phase, the AST involved recovery processes include angiogenesis, synaptogenesis, axogenesis, astrogliosis and neurogenesis. Promoting these processes through potential astrocyte-related targets during this phase may be an effective therapeutic strategy [44].

As an important glutamate receptor in the brain, mGluR5 is essential for the regulation of glutamate homeostasis and directly affects the onset and treatment of various diseases [45]. A previous study found that in a rat tMCAO model, administration of the selective mGluR5 antagonist 2-methyl-6-phenylethynylpyridine (MPEP) and the selective mGluR5 agonist (R,S)-2-chloro-5-hydroxyphenylglycine (CHPG) into the lateral ventricle could both reduce the infarction volumes. The neuroprotective effect of CHPG and MPEP was dose dependent. In addition, MPEP could serve as a noncompetitive NMDA antagonist and an mGluR5 antagonist to block agonist-induced phosphoinositide hydrolysis; in contrast, the neuroprotective effect of CHPG was more due to its antiapoptotic activity [46]. Studies have shown that there is a macromolecular complex formed by AQP4/Na^+, K^+-ATPase/mGluR5 on primary cultured ASTs obtained from normal rat striatum, which can regulate water and K^+ steady state and is involved in the regulation of neuron-astrocyte metabolic crosstalk [47]. A previous study also suggested that AQP4 activation was closely related to glutamate-induced AST swelling by activating mGluR5 [24]. The current study confirmed that MB can reduce the expression of mGluR5 in a model of ischemia-reperfusion brain edema both *in vivo* and *in vitro*. In addition, it validated that MB could reduce the AST swelling *in vitro* caused by the mGluR5 agonist DHPG, which is similar to the effects of fenobam (a selective mGluR5 antagonist), indicating that the effect of MB on AST swelling and AQP4 expression was directly dependent on mGluR5 activation.

Osmotherapy, such as hypertonic saline and mannitol, is the most routine method used clinically to treat intracranial hypertension as well as cerebral edema. Numerous retrospective and prospective series have confirmed that intravenous administration of hypertonic saline or mannitol lowers intracranial pressure by creating osmotic disequilibrium between the intracellular and extracellular compartments, which leads to water moving into the extracellular compartment to restore equilibrium [48]. A recent study also suggested that hypertonic saline could improve brain edema resulting from TBI by suppressing the NF-κB/IL-1β signaling pathway and AQP4 [49]. However, administration of any hypertonic solution would produce a shift of water into the extracellular and intravascular

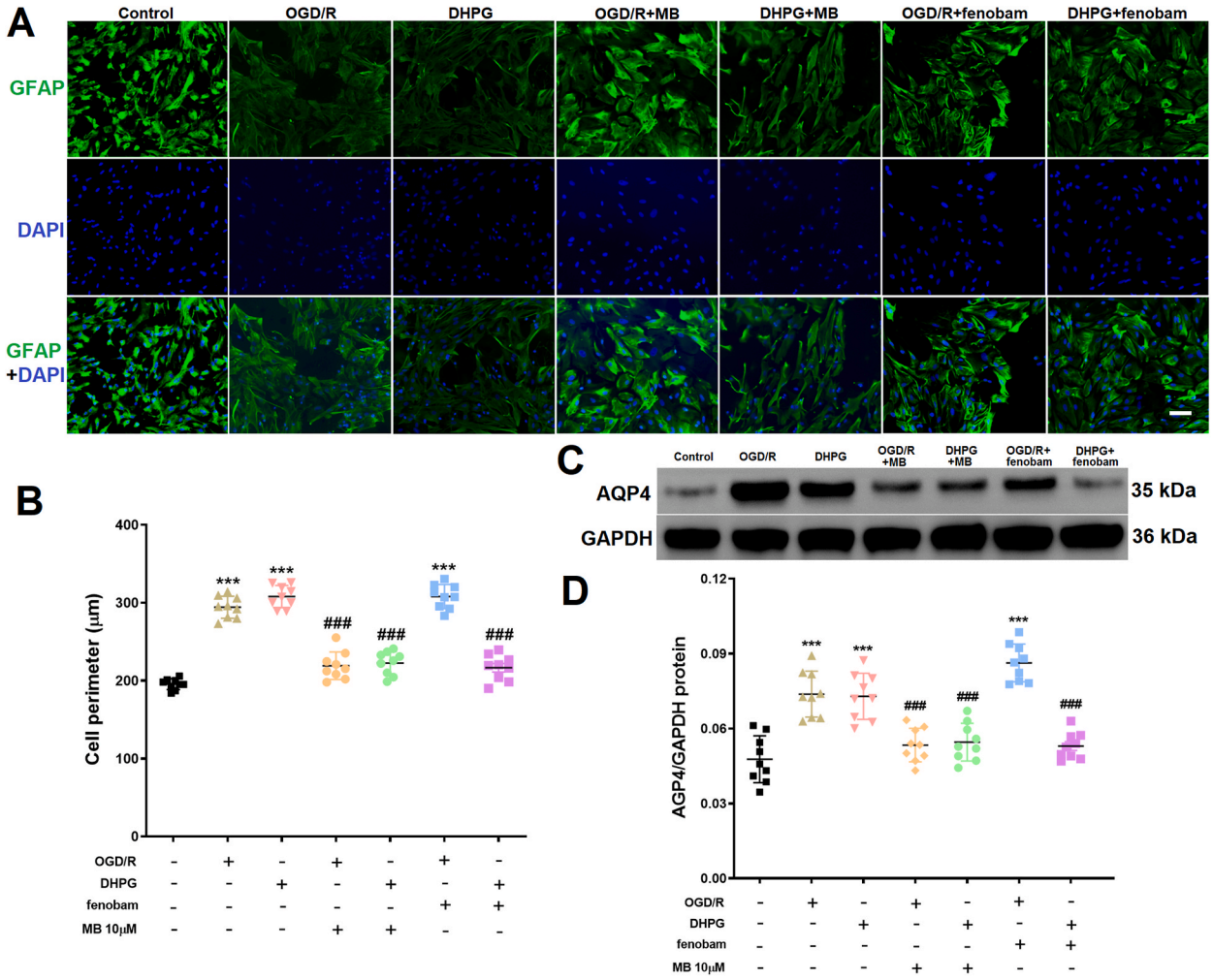

Fig. 10. The effect of MB on astrocyte swelling and AQP4 (regulation of mGluR5). (A). immunofluorescence staining for GFAP in cultured astrocytes. Scale bars show 50 μm. (B). Astrocyte perimeters in each group measured according to Panel (A). Ten cells in each field under high magnification (200 ×) were randomly selected. Three fields in three wells were measured in every group, and the values of nine fields were calculated as the cell perimeter of each group. (C). AQP4 protein expression in each group determined through Western blotting. (D). Quantitative analysis of AQP4 protein expression in each group. All results are obtained on the basis of 3 repeated independent samples which were repeated for 3 times. All data are shown as the mean ± SD, *p < 0.05 vs. control.

spaces, which could increase the blood volume, lead to increased cardiac load and blood pressure and even cause acute left ventricular failure [50]. In contrast to osmotherapy, recent studies more focus on the targeted modulation of AQPs and various techniques such as video microscopy, light scattering and fluorescence quenching have been used to test putative AQP inhibitors in both AQP-expressing mammalian cells and heterologous expression systems [51]. Evidence from a wide variety of studies now supports a view of the functions of AQPs being much more complex than simply mediating the passive flow of water across biological membranes [52]. Given the difficulties in developing pore-blocking AQP4 inhibitors, there is no aquaporin-targeted drug in the clinic and AQPs have been perceived to be intrinsically non-druggable targets [5]. It is suggested that discovery and development of small-molecule AQP inhibitors targetting the trafficking of AQP proteins to the plasma membrane could be one viable alternative drug target to direct inhibition of the water-conducting pore [53]. The current study highlighted that the anti-edema effect of MB was mainly achieved by modulating mGluR5 and AQP4 expression. Considering the neuroprotective effect of MB, it has the potential to be a dual-target agent for the clinical treatment of ischemic stroke.

MB is a well-established drug with a long history of use owing to its diverse range of use and its minimal side effect profile when at low doses [54]. Although, the present study showed the regulatory effect of MB on AQP4 and mGluR5 expression in an ischemic stroke model. There are still some limitations of the current study. First, more precise assay method, such as Sholl analysis from Chiu et al. [55], is needed to capture the AST morphology changes following OGD/R. Second, we only use single dose MB administration for one time before reperfusion to evaluate the protective effect on tMCAO rats. Future studies will more focus on the chronic administration of MB in different doses and administration method to get better neuroprotective effect. Third, DHPG alone could induce ASTs swelling,

which could be attenuated by MB treatment. However, more studies were still needed to focus on the direct regulatory target of MB on AQP4 and/or mGluR5 in brain edema and the impact of DHPG on the anti-swelling effect of MB on OGD/Re-induced AST swelling as well as the regulatory role on AQP4. Meanwhile, brain edema is a severe complication of different types of cerebral diseases, such as traumatic brain injuries (TBI), stroke and gliomas. Due to the polarized expression and localization of AQP4 at the astrocytes endfeet, the 3D *in vitro* models are essential for future studies. The use of humanized self-organized models, organoids, 3D cultures and human microvessel-on-a-chip platforms especially those which are amenable for advanced imaging such as transmission electron microscopy (TEM) and expansion microscopy since they enable real-time monitoring and will be a powerful tool for targeted drug discovery [56,57]. The increased AQP4 expression and the redistribution/surface localization can be two different concepts. Previous studies have shown an increased in AQP4 membrane localization in primary human astrocytes which wasn't accompanied by a change in AQP4 protein expression levels [58,59]. This mislocalization can be a potential therapeutic target [60].

In conclusion, the present study demonstrated the therapeutic effects of MB on tMCAO-induced brain edema in a rat tMCAO model and found that AQP4 and mGluR5 expression was upregulated in the model group, which was reversed by MB treatment. The *in vitro* study also showed that MB could ameliorate OGD/R-induced AST swelling by downregulating AQP4 and mGluR5 expression. Furthermore, MB could reduce the AST swelling caused by the mGluR5 agonist DHPG, which is similar to the effects of fenobam (a selective mGluR5 antagonist), indicating that the effect of MB on AST swelling and AQP4 expression was directly dependent on mGluR5 inhibition *in vitro*. AQP4 has been validated as an important drug target to regulate the CNS water homeostasis, but there is no single drug that has yet been approved to successfully target it for therapeutic use [5,38,51]. Our current study provides essential experimental evidence for alternative routes of targeting AQP function compared to the traditional pore-blocking approach.

Data availability statement

Data will be made on request.

Funding statement

This work has supported by Hebei Provincical Department of Science and Technology (No 172777100D).

Ethical approval

The study protocol received approval from the Animal Care and Use Committee at Beijing Neurosurgical Institute (No. 201401007). The current study was carried out at Beijing Neurosurgical Institute. Animal intervention procedure was performed according to the National Institutes of Health – Office of Laboratory Animal Welfare policies and laws. All animal studies were complied with the ARRIVE guidelines.

CRediT authorship contribution statement

Yu Lai: Writing – review & editing, Writing – original draft, Methodology, Funding acquisition, Conceptualization. **Jie Han:** Data curation. **Dongxian Qiu:** Formal analysis. **Xinyan Liu:** Investigation. **Kan Sun:** Resources. **Yuzhu Fan:** Supervision, Software. **Chunliang Wang:** Visualization, Validation. **Song Zhang:** Writing – review & editing, Project administration.

Declaration of competing interest

The authors declare that they have no known competing financial interests or personal relationships that could have appeared to influence the work reported in this paper.

Acknowledgments

We thank Prof. Xu Yan from Beijing Neurosurgical Institute for his great help regarding our experiments.

Appendix A. Supplementary data

Supplementary data to this article can be found online at https://doi.org/10.1016/j.heliyon.2024.e29483.

References

[1] Y. Yao, Y. Zhang, X. Liao, R. Yang, Y. Lei, J. Luo, Potential therapies for cerebral edema after ischemic stroke: a mini review, Front. Aging Neurosci. 12 (2021) 618819.
[2] B.T. Assefa, A.K. Gebre, B.M. Altaye, Reactive astrocytes as drug target in Alzheimer's disease, BioMed Res. Int. 2018 (2018).

[3] M. Mamtilahun, G. Tang, Z. Zhang, Y. Wang, Y. Tang, G.-Y. Yang, Targeting water in the brain: role of aquaporin-4 in ischemic brain edema, Curr. Drug Targets 20 (2019) 748–755.
[4] H. Chu, C. Huang, H. Ding, J. Dong, Z. Gao, X. Yang, Y. Tang, Q. Dong, Aquaporin-4 and cerebrovascular diseases, Int. J. Mol. Sci. 17 (2016) 1249.
[5] M.M. Salman, P. Kitchen, A. Halsey, M.X. Wang, S. Törnroth-Horsefield, A.C. Conner, J. Badaut, J.J. Iliff, R.M. Bill, Emerging roles for dynamic aquaporin-4 subcellular relocalization in CNS water homeostasis, Brain 145 (2021) 64–75.
[6] A.R. Malik, T.E. Willnow, Excitatory amino acid transporters in physiology and disorders of the central nervous system, Int. J. Mol. Sci. 20 (2019) 5671.
[7] A. Reiner, J. Levitz, Glutamatergic signaling in the central nervous system: ionotropic and metabotropic receptors in concert, Neuron 98 (2018) 1080–1098.
[8] C.-Y. Liu, J.-B. Chen, Y.-Y. Liu, X.-M. Zhou, M. Zhang, Y.-M. Jiang, Q.-Y. Ma, Z. Xue, Z.-Y. Zhao, X.-J. Li, J.-X. Chen, Saikosaponin D exerts antidepressant effect by regulating Homer1-mGluR5 and mTOR signaling in a rat model of chronic unpredictable mild stress, Chin. Med. 17 (2022) 60.
[9] M. Paquet, F.M. Ribeiro, J. Guadagno, J.L. Esseltine, S.S. Ferguson, S.P. Cregan, Role of metabotropic glutamate receptor 5 signaling and homer in oxygen glucose deprivation-mediated astrocyte apoptosis, Mol. Brain 6 (2013) 1–11.
[10] N. Abreu, A. Acosta-Ruiz, G. Xiang, J. Levitz, Mechanisms of differential desensitization of metabotropic glutamate receptors, Cell Rep. 35 (2021) 109050.
[11] A.A. Kritis, E.G. Stamoula, K.A. Paniskaki, T.D. Vavilis, Researching glutamate – induced cytotoxicity in different cell lines: a comparative/collective analysis/study, Front. Cell. Neurosci. 9 (2015).
[12] Markou A, Kitchen P, Aldabbagh A, Repici M, Salman MM, Bill RM and Balklava Z. Mechanisms of aquaporin-4 vesicular trafficking in mammalian cells. J. Neurochem. n/a:.
[13] E. Gunnarson, M. Zelenina, G. Axehult, Y. Song, A. Bondar, P. Krieger, H. Brismar, S. Zelenin, A. Aperia, Identification of a molecular target for glutamate regulation of astrocyte water permeability, Glia 56 (2008) 587–596.
[14] S. Scheindlin, Something old... something blue, Mol. Interv. 8 (2008) 268.
[15] M. Alda, Methylene blue in the treatment of neuropsychiatric disorders, CNS Drugs 33 (2019) 719–725.
[16] E. Poteet, A. Winters, L.-J. Yan, K. Shufelt, K.N. Green, J.W. Simpkins, Y. Wen, S.-H. Yang, Neuroprotective actions of methylene blue and its derivatives, PLoS One 7 (2012) e48279.
[17] M.M. Salman, P. Kitchen, M.N. Woodroofe, R.M. Bill, A.C. Conner, P.R. Heath, M.T. Conner, Transcriptome analysis of gene expression provides new insights into the effect of mild therapeutic hypothermia on primary human cortical astrocytes cultured under hypoxia, Front. Cell. Neurosci. 11 (2017).
[18] M.M. Salman, M.A. Sheilabi, D. Bhattacharyya, P. Kitchen, A.C. Conner, R.M. Bill, M.N. Woodroofe, M.T. Conner, A.P. Princivalle, Transcriptome analysis suggests a role for the differential expression of cerebral aquaporins and the MAPK signalling pathway in human temporal lobe epilepsy, Eur. J. Neurosci. 46 (2017) 2121–2132.
[19] Z-f Shi, Q. Fang, Y. Chen, L-x Xu, M. Wu, M. Jia, Y. Lu, X-x Wang, Y-j Wang, X. Yan, Methylene blue ameliorates brain edema in rats with experimental ischemic stroke via inhibiting aquaporin 4 expression, Acta Pharmacol. Sin. 42 (2021) 382–392.
[20] Q. Fang, X. Yan, S. Li, Y. Sun, L. Xu, Z. Shi, M. Wu, Y. Lu, L. Dong, R. Liu, Methylene blue ameliorates ischemia/reperfusion-induced cerebral edema: an MRI and transmission electron microscope study, in: Brain Edema XVI, Springer, 2016, pp. 227–236.
[21] Y. Chen, B. Yang, L. Xu, Z. Shi, R. Han, F. Yuan, J. Ouyang, X. Yan, K.K. Ostrikov, Inhalation of atmospheric-pressure gas plasma attenuates brain infarction in rats with experimental ischemic stroke, Front. Neurosci. 16 (2022) 875053.
[22] T. Gerriets, E. Stolz, M. Walberer, C. Muller, A. Kluge, A. Bachmann, M. Fisher, M. Kaps, G. Bachmann, Noninvasive quantification of brain edema and the space-occupying effect in rat stroke models using magnetic resonance imaging, Stroke 35 (2004) 566–571.
[23] Y. Xu, Z.F. Shi, L.X. Xu, J.X. Li, W. Min, X.X. Wang, J. Mei, L.P. Dong, S.H. Yang, Y. Fang, Glutamate impairs mitochondria aerobic respiration capacity and enhances glycolysis in cultured rat astrocytes, Biomed. Environ. Sci. 30 (2017) 44–51.
[24] Z. Shi, W. Zhang, Y. Lu, Y. Lu, L. Xu, Q. Fang, M. Wu, M. Jia, Y. Wang, L. Dong, Aquaporin 4-mediated glutamate-induced astrocyte swelling is partially mediated through metabotropic glutamate receptor 5 activation, Front. Cell. Neurosci. 11 (2017) 116.
[25] K.C. Biju, R.C. Evans, K. Shrestha, D.C.B. Carlisle, J. Gelfond, R.A. Clark, Methylene blue ameliorates olfactory dysfunction and motor deficits in a chronic MPTP/probenecid mouse model of Parkinson's disease, Neuroscience 380 (2018) 111–122.
[26] V. Paban, C. Manrique, M. Filali, S. Maunoir-Regimbal, F. Fauvelle, B. Alescio-Lautier, Therapeutic and preventive effects of methylene blue on Alzheimer's disease pathology in a transgenic mouse model, Neuropharmacology 76 (2014) 68–79.
[27] H. Atamna, R. Kumar, Protective role of methylene blue in Alzheimer's disease via mitochondria and cytochrome c oxidase, J Alzheimers Dis 20 (2010) S439–S452.
[28] M.G. Ryou, G.R. Choudhury, W. Li, A. Winters, F. Yuan, R. Liu, S.H. Yang, Methylene blue-induced neuronal protective mechanism against hypoxia-reoxygenation stress, Neuroscience 301 (2015) 193–203.
[29] M.C. Papadopoulos, S. Krishna, A. Verkman, Aquaporin water channels and brain edema, The Mount Sinai journal of medicine, New York 69 (2002) 242–248.
[30] A. Xiong, J. Li, R. Xiong, Y. Xia, X. Jiang, F. Cao, H. Lu, J. Xu, F. Shan, Inhibition of HIF-1α-AQP4 axis ameliorates brain edema and neurological functional deficits in a rat controlled cortical injury (CCI) model, Sci. Rep. 12 (2022) 1–9.
[31] Y. Wang, C. Huang, Q. Guo, H. Chu, Aquaporin-4 and cognitive disorders, Aging Dis 13 (2022) 61.
[32] A.K. Azad, T. Raihan, J. Ahmed, A. Hakim, T.H. Emon, P.A. Chowdhury, Human aquaporins: functional diversity and potential roles in infectious and non-infectious diseases, Front. Genet. 12 (2021) 654865.
[33] P. Kitchen, M.M. Salman, A.M. Halsey, C. Clarke-Bland, J.A. MacDonald, H. Ishida, H.J. Vogel, S. Almutiri, A. Logan, S. Kreida, T. Al-Jubair, J. Winkel Missel, P. Gourdon, S. Törnroth-Horsefield, M.T. Conner, Z. Ahmed, A.C. Conner, R.M. Bill, Targeting aquaporin-4 subcellular localization to treat central nervous system edema, Cell 181 (2020) 784–799.e719.
[34] N.J. Sylvain, M.M. Salman, M.J. Pushie, H. Hou, V. Meher, R. Herlo, L. Peeling, M.E. Kelly, The effects of trifluoperazine on brain edema, aquaporin-4 expression and metabolic markers during the acute phase of stroke using photothrombotic mouse model, Biochim. Biophys. Acta Biomembr. 1863 (2021) 183573.
[35] G.T. Manley, M. Fujimura, T. Ma, N. Noshita, F. Filiz, A.W. Bollen, P. Chan, A. Verkman, Aquaporin-4 deletion in mice reduces brain edema after acute water intoxication and ischemic stroke, Nat. Med. 6 (2000) 159–163.
[36] M.J. Tait, S. Saadoun, B.A. Bell, A.S. Verkman, M.C. Papadopoulos, Increased brain edema in aqp4-null mice in an experimental model of subarachnoid hemorrhage, Neuroscience 167 (2010) 60–67.
[37] P. Kitchen, M.M. Salman, M. Abir-Awan, T. Al-Jubair, S. Törnroth- Horsefield, A.C. Conner, R.M. Bill, Calcein fluorescence quenching to measure plasma membrane water flux in live mammalian cells, STAR Protocols 1 (2020) 100157.
[38] M.M. Salman, P. Kitchen, A.J. Yool, R.M. Bill, Recent breakthroughs and future directions in drugging aquaporins, Trends Pharmacol. Sci. 43 (2022) 30–42.
[39] A. Verkhratsky, A. Butt, B. Li, P. Illes, R. Zorec, A. Semyanov, Y. Tang, M.V. Sofroniew, Astrocytes in human central nervous system diseases: a frontier for new therapies, Signal Transduct. Targeted Ther. 8 (2023) 396.
[40] M. Pekny, M. Pekna, Astrocyte reactivity and reactive astrogliosis: costs and benefits, Physiol. Rev. 94 (2014) 1077–1098.
[41] R.M. Jha, P.M. Kochanek, J.M. Simard, Pathophysiology and treatment of cerebral edema in traumatic brain injury, Neuropharmacology 145 (2019) 230–246.
[42] W. Han, Y. Song, M. Rocha, Y. Shi, Ischemic brain edema: emerging cellular mechanisms and therapeutic approaches, Neurobiol. Dis. 178 (2023) 106029.
[43] Y. Gu, C. Zhou, Z. Piao, H. Yuan, H. Jiang, H. Wei, Y. Zhou, G. Nan, X. Ji, Cerebral edema after ischemic stroke: pathophysiology and underlying mechanisms, Front. Neurosci. 16 (2022).
[44] Alhadidi QM, Bahader GA, Arvola O, Kitchen P, Shah ZA and Salman MM. Astrocytes in functional recovery following central nervous system injuries. J. Physiol. n/a:. .
[45] D.O. Borroto-Escuela, A.O. Tarakanov, I. Brito, K. Fuxe, Glutamate heteroreceptor complexes in the brain, Pharmacol. Rep. 70 (2018) 936–950.
[46] W. Bao, A. Williams, A. Faden, F. Tortella, Selective mGluR5 receptor antagonist or agonist provides neuroprotection in a rat model of focal cerebral ischemia, Brain Res. 922 (2001) 173–179.
[47] N. Illarionova, E. Gunnarson, Y. Li, H. Brismar, A. Bondar, S. Zelenin, A. Aperia, Functional and molecular interactions between aquaporins and Na, K-ATPase, Neuroscience 168 (2010) 915–925.

[48] H.E. Hinson, D. Stein, K.N. Sheth, Hypertonic saline and mannitol therapy in critical care neurology, J. Intensive Care Med. 28 (2013) 3–11.
[49] H. Zhang, J. Liu, Y. Liu, C. Su, G. Fan, W. Lu, L. Feng, Hypertonic saline improves brain edema resulting from traumatic brain injury by suppressing the NF-κB/IL-1β signaling pathway and AQP4, Exp. Ther. Med. 20 (2020), 1-1.
[50] M.N. Diringer, The evolution of the clinical use of osmotic therapy in the treatment of cerebral edema, Acta Neurochir. Suppl. 121 (2016) 3–6.
[51] M. Abir-Awan, P. Kitchen, M.M. Salman, M.T. Conner, A.C. Conner, R.M. Bill, Inhibitors of mammalian aquaporin water channels, Int. J. Mol. Sci. 20 (2019).
[52] K. Wagner, L. Unger, M.M. Salman, P. Kitchen, R.M. Bill, A.J. Yool, Signaling mechanisms and pharmacological modulators governing diverse aquaporin functions in human health and disease, Int. J. Mol. Sci. 23 (2022) 1388.
[53] A. Markou, L. Unger, M. Abir-Awan, A. Saadallah, A. Halsey, Z. Balklava, M. Conner, S. Törnroth-Horsefield, S.D. Greenhill, A. Conner, Molecular mechanisms governing aquaporin relocalisation, Biochim. Biophys. Acta Biomembr. 1864 (2022) 183853.
[54] D. Tucker, Y. Lu, Q. Zhang, From mitochondrial function to neuroprotection—an emerging role for methylene blue, Mol. Neurobiol. 55 (2018) 5137–5153.
[55] K.B. Chiu, K.M. Lee, K.N. Robillard, A.G. MacLean, A method to investigate astrocyte and microglial morphological changes in the aging brain of the rhesus macaque, Methods Mol. Biol. 1938 (2019) 265–276.
[56] M.M. Salman, G. Marsh, I. Kusters, M. Delincé, G. Di Caprio, S. Upadhyayula, G. de Nola, R. Hunt, K.G. Ohashi, T. Gray, F. Shimizu, Y. Sano, T. Kanda, B. Obermeier, T. Kirchhausen, Design and validation of a human brain endothelial microvessel-on-a-chip open microfluidic model enabling advanced optical imaging, Front. Bioeng. Biotechnol. 8 (2020).
[57] N.R. Wevers, D.G. Kasi, T. Gray, K.J. Wilschut, B. Smith, R. van Vught, F. Shimizu, Y. Sano, T. Kanda, G. Marsh, S.J. Trietsch, P. Vulto, H.L. Lanz, B. Obermeier, A perfused human blood-brain barrier on-a-chip for high-throughput assessment of barrier function and antibody transport, Fluids Barriers CNS 15 (2018) 23.
[58] P. Kitchen, R.E. Day, L.H.J. Taylor, M.M. Salman, R.M. Bill, M.T. Conner, A.C. Conner, Identification and molecular mechanisms of the rapid tonicity-induced relocalization of the aquaporin 4 channel, J. Biol. Chem. 290 (2015) 16873–16881.
[59] S. Ciappelloni, D. Bouchet, N. Dubourdieu, E. Boué-Grabot, B. Kellermayer, C. Manso, R. Marignier, S.H.R. Oliet, T. Tourdias, L. Groc, Aquaporin-4 surface trafficking regulates astrocytic process motility and synaptic activity in health and autoimmune disease, Cell Rep. 27 (2019) 3860–3872.e3864.
[60] M.M. Salman, P. Kitchen, M.N. Woodroofe, J.E. Brown, R.M. Bill, A.C. Conner, M.T. Conner, Hypothermia increases aquaporin 4 (AQP4) plasma membrane abundance in human primary cortical astrocytes via a calcium/transient receptor potential vanilloid 4 (TRPV4)- and calmodulin-mediated mechanism, Eur. J. Neurosci. 46 (2017) 2542–2547.